






Cite this: *Phys. Chem. Chem. Phys.*,
2021, 23, 1943

Complexity of a peroxidase–oxidase reaction model†

Jason A. C. Gallas, ^{ab} Marcus J. B. Hauser ^c and Lars F. Olsen ^{*d}

The peroxidase–oxidase oscillating reaction was the first (bio)chemical reaction to show chaotic behaviour. The reaction is rich in bifurcation scenarios, from period-doubling to peak-adding mixed mode oscillations. Here, we study a state-of-the-art model of the peroxidase–oxidase reaction. Using the model, we report systematic numerical experiments exploring the impact of changing the enzyme concentration on the dynamics of the reaction. Specifically, we report high-resolution phase diagrams predicting and describing how the reaction unfolds over a quite extended range of enzyme concentrations. Surprisingly, such diagrams reveal that the enzyme concentration has a huge impact on the reaction evolution. The highly intricate dynamical behaviours predicted here are difficult to establish theoretically due to the total absence of an adequate framework to solve nonlinearly coupled differential equations. But such behaviours may be validated experimentally.

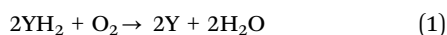
Received 26th November 2020,
Accepted 6th January 2021

DOI: 10.1039/d0cp06153k

rsc.li/pccp

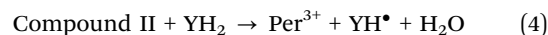
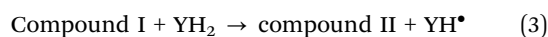
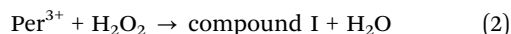
1 Introduction

The peroxidase–oxidase (PO) reaction is the oxidation of an organic donor (YH₂) with molecular oxygen as the electron acceptor. The reaction is catalyzed by the enzyme peroxidase

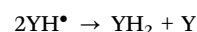


The electron donor used in reaction (1) may be a number of small organic molecules or reduced nicotinamide dinucleotide (NADH).^{1,2}

Many peroxidases are heme enzymes.¹ The catalytic cycle of the PO reaction is quite complex and involves five different oxidation states of the heme in the enzyme: ferrous peroxidase and ferric peroxidase, which differ in the oxidation state of the heme iron, and compound I, compound II and compound III, which are different oxygen-binding forms of the enzyme, that are characterized by having oxidation states of +5, +4 and +6, respectively. In native peroxidase the iron is in the Fe³⁺ state. Ferric peroxidase (Per³⁺), compound I and compound II participate in the peroxidase catalytic cycle:



The free radicals (YH[•]) formed in this cycle may disproportionate



or form a dimer (YH)₂. In addition to the peroxidase catalytic cycle (eqn (2)–(4)) the PO reaction involves a number of non-enzymatic free-radical reactions (reactions and radical reactions involving the enzyme). Some of these reactions are listed below in Table 1. A more detailed list of reactions known or believed to participate in the PO reaction can be found in ref. 2.

With a continuous supply of NADH and in the presence of a modifier (phenol or related compound⁴) the reaction is known to display a rich variety of dynamic behaviours, ranging from bistability⁶ to oscillations,^{7–10} and to chaos.¹¹ In fact, the discovery of chaos in the PO reaction was made shortly after the publication in 1976 of a seminal paper by Otto Rössler,¹² thereby demonstrating for the first time that a mathematical model of a (bio)chemical reaction could display such behaviour. Shortly thereafter, chaos was also found in the Belousov–Zhabotinsky (BZ) reaction.^{13,14} Since then chaos and other complex dynamics have been observed in several (bio)chemical reaction systems.¹⁵

Because of this abundance of diverse complex behaviours the PO reaction has developed into an important biochemical reaction system, which has influenced the search for similar complexity in numerous other biological systems. Here we wish to, first, present some experimental observations of complex

^a Instituto de Altos Estudos da Paraíba, Rua Silvino Lopes 419-2502, 58039-190 João Pessoa, Brazil

^b Complexity Sciences Center, 9225 Collins Avenue Suite 1208, Surfside, FL 33154-3001, USA

^c Department of Regulation Biology, Institute of Biology, Otto-von-Guericke Universität Magdeburg, Pöfänger Platz 5, 39106 Magdeburg, Germany

^d PhyLife, Institute of Biochemistry and Molecular Biology, University of Southern Denmark, Campusvej 55, DK-5230 Odense M, Denmark. E-mail: lfo@bmb.sdu.dk

† Electronic supplementary information (ESI) available. See DOI: 10.1039/d0cp06153k

Table 1 List of reactions, rate expressions and rate constants for the BFSO model (adapted from Bronnikova *et al.*¹⁶). In reactions (1)–(11), second-order rate constants have units of $M^{-1} s^{-1}$, while the first-order rate constant in reaction (13) has units of s^{-1} and the zero-order rate constant in reaction (12) has units of $M s^{-1}$. In reaction (13), $[O_2]_{eq} = 12 \times 10^{-6} M$. Per^{n+} refers to the oxidation state of peroxidase: Per^{2+} , ferrous peroxidase; Per^{3+} , ferric peroxidase; Per^{4+} , compound II; Per^{5+} , compound I; Per^{6+} , compound III. Note that the activity of H^+ is absorbed into the rate constant. The last row in the table lists the range of variable rate constants

Reaction	Rate expression	Rate constant	Range
(1) $NADH + H^+ + O_2 \rightarrow NAD^+ + H_2O_2$	$k_1[NADH][O_2]$	3.0	—
(2) $H_2O_2 + Per^{3+} \rightarrow H_2O + Per^{5+}$	$k_2[H_2O_2][Per^{3+}]$	1.8×10^7	—
(3) $Per^{5+} + NADH \rightarrow Per^{4+} + NAD^{\bullet}$	$k_3[Per^{5+}][NADH]$	4.0×10^4	—
(4) $Per^{4+} + NADH \rightarrow Per^{3+} + NAD^{\bullet}$	$k_4[Per^{4+}][NADH]$	2.6×10^4	—
(5) $NAD^{\bullet} + O_2 \rightarrow NAD^+ + O_2^-$	$k_5[NAD^{\bullet}][O_2]$	2.0×10^7	—
(6) $O_2^- + Per^{3+} \rightarrow Per^{6+}$	$k_6[O_2^-][Per^{3+}]$	1.7×10^7	—
(7) $2O_2^- + 2H^+ \rightarrow O_2 + H_2O_2$	$k_7[O_2^-]^2$	2.0×10^7	—
(8) $Per^{6+} + NAD^{\bullet} \rightarrow Per^{5+} + NAD^+$	$k_8[Per^{6+}][NAD^{\bullet}]$	9.0×10^7	—
(9) $2NAD^{\bullet} \rightarrow NAD_2$	$k_9[NAD^{\bullet}]^2$	variable	$0-1 \times 10^8$
(10) $Per^{3+} + NAD^{\bullet} \rightarrow Per^{2+} + NAD^+$	$k_{10}[Per^{3+}][NAD^{\bullet}]$	1.8×10^6	—
(11) $Per^{2+} + O_2 \rightarrow Per^{6+}$	$k_{11}[Per^{2+}][O_2]$	1.0×10^5	—
(12) $\rightarrow NADH$	k_{12}	variable	$1.0 \times 10^{-7}-1.4 \times 10^{-7}$
(13) $O_2(gas) \rightleftharpoons O_2(liquid)$	$k_{13}([O_2]_{eq}-[O_2])$	6.0×10^{-3}	—

dynamics in the experimental system and the organization of the different periodic and chaotic states in a 2D phase space spanned by pH in the reaction mixture and the infusion rate of NADH. Next, we describe in some detail a realistic model of the PO reaction, the Bronnikova–Fedkina–Schaffer–Olsen (BFSO) model,¹⁶ which is capable of reproducing most of the presented experimental observations. Then, we use isospike^{17–21} stability diagrams to explore the complex behaviours of the model for a hitherto unexplored parameter, namely the initial concentrations of the enzyme. These diagrams show some new and unexpected aspects of the complexity of the PO reaction, namely that the enzyme concentration has a huge effect on the structure of the phase diagrams. This change in structure could not have been predicted by analytical or semi-analytical methods and is difficult to explain due to the total absence of a proper theoretical framework to anticipate the behaviour of nonlinear sets of differential equations.

Although the BFSO model is semiquantitative in nature, *i.e.* only a fraction of the rate constants are known with certainty, it has up to now reproduced essentially all the dynamical behaviors recorded experimentally. Therefore, our endeavour to study the behaviours predicted by the model under hitherto unexplored conditions is driven by our hope of motivating the experimental observation of our predictions described below. It is worth pointing out that several of the complex dynamical behaviours observed experimentally in the PO reaction were first predicted by realistic models of the reaction^{22,23} and we hope the results reported below to continue this trend.

2 Complex behaviour in the PO reaction

As mentioned above, the PO reaction will display both simple periodic⁹ and complex periodic oscillations^{10,24} if both reactants, O_2 and NADH, are supplied to a reaction mixture containing peroxidase and an organic modifier (usually 2,4 dichlorophenol). A brief description of the experimental setup

is provided in the ESI,[†] where we also describe how we maintain a constant volume of the reaction mixture by having a low influx rate of NADH stock solution, which is balanced by evaporation of liquid. Some of these complex oscillations belong to a special class of so-called mixed mode oscillations (MMOs), which are oscillations composed of one or more large amplitude peaks with intercalation of one or more small amplitude peaks. To characterize MMOs we use a symbolic notation L^S , where L denotes the number of large peaks and S denotes the number of small peaks in one oscillation period.^{3,24–26} In such regimes, oscillations of medium amplitude are absent. Frequently, MMOs are found in parameter domains where the dynamics change from periodic oscillations to chaos and neighboring MMO states L^S and L^{S+1} are often separated by narrow windows with chaotic dynamics. However, Hauck and Schneider²⁴ observed a sequence of L^S states in the PO reaction that apparently were not separated by such windows of chaotic dynamics. An example of a MMO peak-adding scenario is shown in Fig. 1.

This figure shows a sequence of oscillations of compound III (oxyferrous peroxidase), which has an absorption maximum at 418 nm, following increases in the mean NADH concentration (mediated by changes in NADH infusion rate). The sequence of MMO states as the average concentration of NADH is gradually increased is 1^0 (blue) $\rightarrow 1^1$ (green) $\rightarrow 1^2$ (cyan) $\rightarrow 1^3$ (red) $\rightarrow \dots \rightarrow$ chaos (black). As the average NADH concentration is increased further small amplitude periodic oscillations start in the sequence $\dots \rightarrow 0^4$ (dark red) $\rightarrow 0^2$ (dark green) $\rightarrow 0^1$ (gray). The bifurcation scenario illustrated in Fig. 1 was obtained at a relatively high pH (pH 6.3). If the same experiment is done at a lower pH (*e.g.* pH 5.2) then, instead of peak-adding MMOs, one observes a period doubling scenario.³ Fig. 2 shows a phase diagram of dynamic states spanned by the relative mean concentration of NADH and pH. We note from the figure that at around pH 5.4 there seems to be a crossover of transitions to chaos from period doubling to MMO peak-adding scenarios. We also note from Fig. 2 that at pH 6.3 the transition from the 1^1 periodic state to the 1^2 periodic state is preceded by

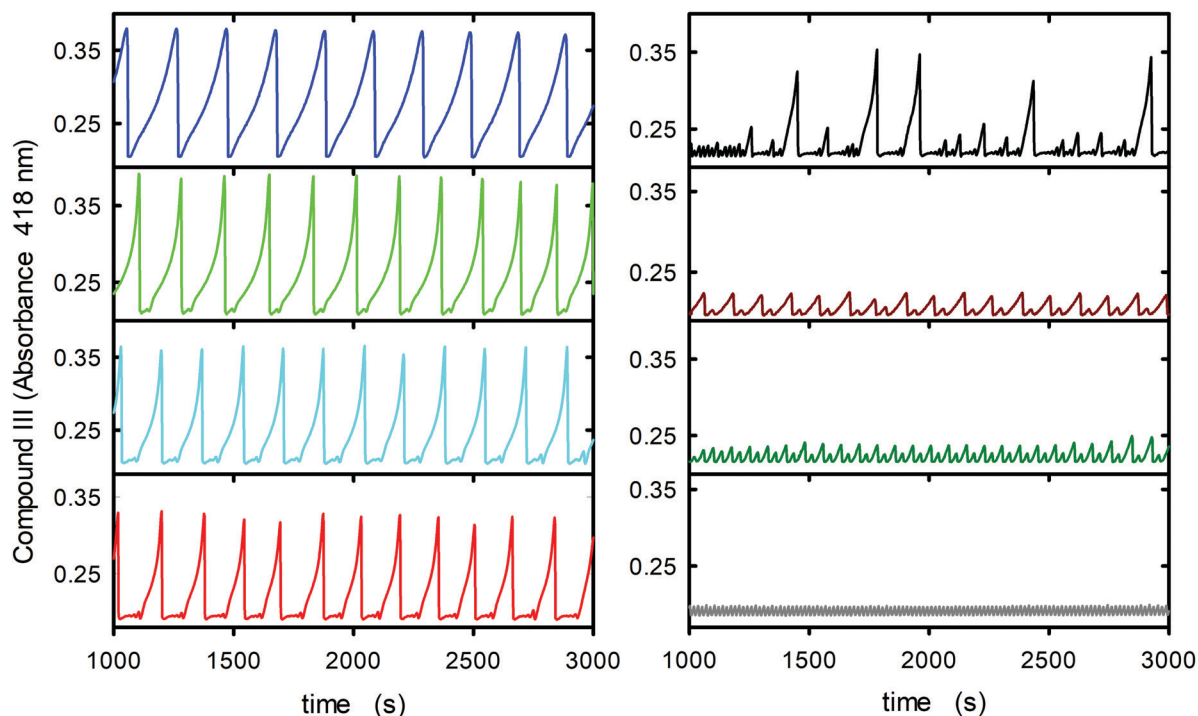


Fig. 1 Experimental data illustrating peak-adding mixed mode scenario in the PO reaction. The figure shows oscillations in the absorption of compound III following progressive increases in the mean NADH concentration (mediated by changes in infusion rate of NADH into the reaction system). The sequence of L^5 states depicted are 1^0 (blue) \rightarrow 1^1 (green) \rightarrow 1^2 (cyan) \rightarrow 1^3 (red) \rightarrow chaos (black) \rightarrow O^4 (dark red) \rightarrow O^2 (dark green) \rightarrow O^1 (gray). Adapted from Hauser *et al.*³

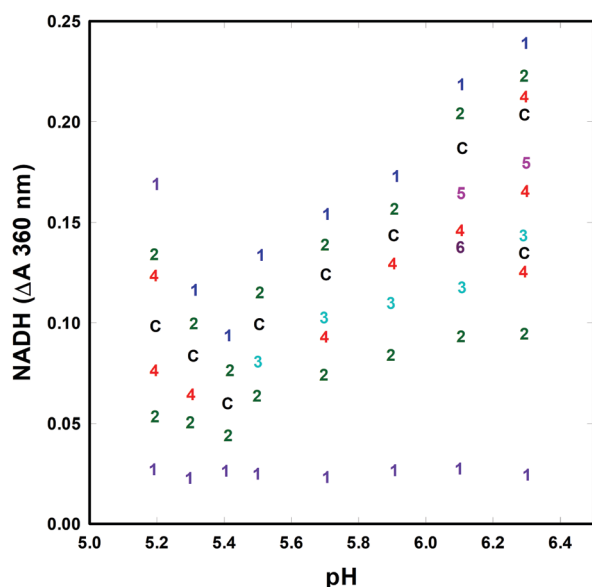


Fig. 2 Experimental phase diagram of the PO reaction spanned by pH and the relative concentration of NADH (determined as the absorption at 360 nm). The latter is indirectly linked to the inflow rate of NADH. The numbers indicate the number of peaks per period; C indicates chaos. Adapted from Hauser *et al.*³

a period-doubled (1^1)² state followed by a narrow chaotic domain. A similar period-doubled (1^1)² state was observed at pH 5.7, but in this case the narrow chaotic domain is either

absent or too narrow to be monitored. Finally, at pH 6.1 a period-doubled (1^2)² state could be determined in the transition from the 1^2 to the 1^3 states. There are undoubtedly many other narrow periodic and non-periodic states that have escaped measurement.

The bifurcation scenarios presented in Fig. 1 and 2 are for an enzyme concentration of 1.5 μ M. However, other and quite different scenarios have been obtained at either higher^{24,25,27} or lower enzyme concentrations.^{10,11} The range of peroxidase concentrations used in experiments ranges from 0.45 μ M^{10,11} to about 5 μ M.^{24,25,27} Nevertheless, a systematic experimental study of the effect of changes in enzyme concentration on the dynamics of the PO reaction has never been done. Such experiments are extremely complex and time consuming but fortunately numerical explorations are feasible and provide clear indications of the exact conditions where it would be desirable and promising to perform additional experimental work.

3 The BFSO model of the PO reaction

The oscillating PO reaction has been simulated using both simple^{10,28} and detailed^{29,31–34} models. While the simple models are capable of exhibiting both period-doubling and MMO scenarios,^{35,36} most of the early detailed models show only bistability and simple periodic oscillations.^{29,31,32,34} An exception is the model Z of Aguda and Larter,³³ which displays a period-doubling cascade to chaos.

A more recent model is the Bronnikova–Fedkina–Schaffer–Olsen (BFSO) model.¹⁶ The BFSO model is not radically different from the detailed models listed above. It has strong connections to the model Z of Aguda and Larter³³ and the so-called Urbanalator.³⁴ The difference to the older models is mainly in the selection of reactions and the choice of rate constants and parameters relating to the inflow of reactants similar to the experimental conditions. The reactions, rate expressions and rate constants of the BFSO model are listed in Table 1. A reaction scheme is presented in Fig. 3. The black reactions in Fig. 3 ensure only periodic oscillations in the model. However, combining the black and the red reactions results in complex periodic oscillations and chaos. Thus, in this case chaos may be regarded as the result of two coupled periodic oscillators.

The BFSO model (Table 1) translates into the following ten coupled differential equations:

$$\frac{dx_1}{dt} = k_2x_4x_{10} - k_3x_1x_6 + k_8x_3x_5, \quad (5)$$

$$\frac{dx_2}{dt} = k_3x_1x_6 - k_4x_2x_6, \quad (6)$$

$$\frac{dx_3}{dt} = -k_8x_3x_5 + k_{11}x_7x_9 + k_6x_8x_{10}, \quad (7)$$

$$\frac{dx_4}{dt} = k_1x_6x_7 + k_7x_8^2 - k_2x_4x_{10}, \quad (8)$$

$$\frac{dx_5}{dt} = k_3x_1x_6 + k_4x_2x_6 - k_5x_5x_7 - k_8x_3x_5 - 2k_9x_5^2 - k_{10}x_5x_{10}, \quad (9)$$

$$\frac{dx_6}{dt} = -k_1x_6x_7 - k_3x_1x_6 - k_4x_2x_6 + k_{12}, \quad (10)$$

$$\frac{dx_7}{dt} = -k_1x_6x_7 - k_5x_5x_7 + k_7x_8^2 - k_{11}x_7x_9 - k_{13}x_7 + k_{13}[\text{O}_2]_{\text{eq}}, \quad (11)$$

$$\frac{dx_8}{dt} = k_5x_5x_7 - 2k_7x_8^2 - k_6x_8x_{10}, \quad (12)$$

$$\frac{dx_9}{dt} = k_{10}x_5x_{10} - k_{11}x_7x_9, \quad (13)$$

$$\frac{dx_{10}}{dt} = -k_2x_4x_{10} + k_4x_2x_6 - k_6x_8x_{10} - k_{10}x_5x_{10}. \quad (14)$$

The correspondence between the variables x_i and chemical species in Table 1 is the following: $x_1 \leftrightarrow \text{Per}^{5+}$, $x_2 \leftrightarrow \text{Per}^{4+}$, $x_3 \leftrightarrow \text{Per}^{6+}$, $x_4 \leftrightarrow \text{H}_2\text{O}_2$, $x_5 \leftrightarrow \text{NAD}^\bullet$, $x_6 \leftrightarrow \text{NADH}$, $x_7 \leftrightarrow \text{O}_2$, $x_8 \leftrightarrow \text{O}_2^-$, $x_9 \leftrightarrow \text{Per}^{2+}$, $x_{10} \leftrightarrow \text{Per}^{3+}$.

It must be highlighted that although the total concentration of the enzyme remains constant, there is a considerable dynamics as to how the different redox states of the enzyme are populated at different points in time. Thus, the conservation relation $x_1 + x_2 + x_3 + x_9 + x_{10} = x_{10}(0)$ is always fulfilled, where $x_{10}(0)$ is the initial concentration of Per^{3+} added to the reaction medium. Due to this conservation relation, the concentration of the enzyme in the medium is not a mere initial condition, but a parameter that will affect the entire dynamics of the reaction system. Numerical solutions of eqn (5)–(14) show the existence of domains of complex and chaotic dynamics which are both rich and intricate.^{3,26,37–41} The numerical simulations reproduce several experimental observations in the PO reaction, *e.g.* that the chaotic domain can be reached either *via* a period-doubling route (at low pH) or a peak-adding (often also called period-adding) route (at higher pH) as the relevant parameter is varied. The latter scenario is associated with the occurrence of relatively narrow chaotic window separating adjacent states of mixed-mode oscillations (MMOs)³ L^S and L^{S+1} . As the bifurcation parameter is continuously varied, the sequence of MMOs progresses by a successive addition of low amplitude oscillations to the MMO states until a relatively broad region of chaotic dynamics is reached.

4 Motivation

Recently, the dynamics of the BFSO model was studied using isospike^{17–21} stability diagrams in the control parameter plane spanned by the supply rate of NADH (reflected by the rate k_{12}) and the pH-dependent dimerisation of NAD radicals (rate constant k_9).⁴¹ Such diagrams represent a powerful way to get an overview of the periodic and non-periodic states in two-dimensional sections of a multi-parameter control parameter space. In addition to a period-doubling route to chaos, which is found for high values of k_9 , an extensive domain of the parameter space is occupied by peak-adding sequences. Interestingly, two types of peak-adding sequences exist, namely a classical peak-adding sequence, where adjacent MMO states are separated by narrow chaotic windows on the one hand, and on the other hand a peak-adding sequence where a L^S state is

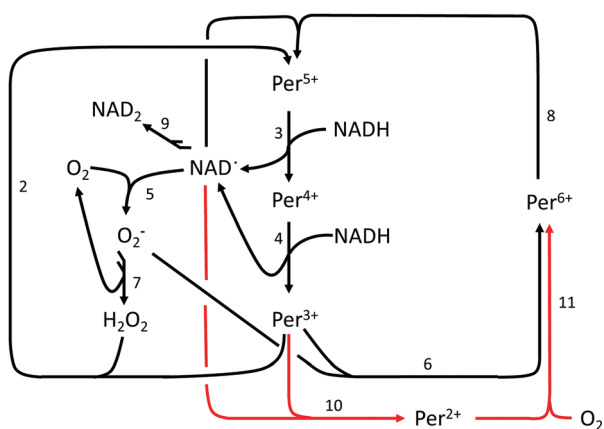


Fig. 3 Reaction scheme of the BFSO model. The black lines with arrow represent the original Urbanalator model,³⁴ while the red lines represent the supplementary reactions in the BFSO model. The numbers refer to the reactions in Table 1. For clarity the reactions (1), (12) and (13) in Table 1 have been omitted from the scheme. Note that the black reactions provide for only simple oscillations. Complex dynamics implies participation of the red reactions. Adapted from Hauser and Olsen.⁵

converted to a L^{S+1} state by the simple addition of a low-amplitude oscillation to the MMO. The latter scenario is referred to as non-chaos mediated MMOs.⁴¹ Both scenarios, chaos-mediated and non-chaos mediated MMOs have been reported experimentally.^{24,26} In addition to reproducing experimentally observed dynamic behaviours, the extensive numerical study of the BFSO model by Hauser and Gallas⁴¹ following changes in parameters k_9 and k_{12} revealed new dynamic behaviours, which awaits experimental verification. For example, a new compact domain of complex and non-periodic dynamics was found at relatively high values of k_{12} and low values of k_9 . This domain is characterized by an intricate mosaic of periodic windows intercalated by domains of chaotic dynamics. These chaotic domains display a peculiar fault running through them.⁴¹

Motivated by the study of Hauser and Gallas⁴¹ and the lack of experimental knowledge how the enzyme concentration may affect the dynamics of the PO reaction we have used isospike stability diagrams to study the dynamics of the BFSO model for different initial concentrations of variable x_{10} ($[\text{Per}^{3+}]$). As a reference point we use the experimental studies presented in Fig. 1 and 2 that were conducted with an enzyme concentration of 1.5 μM and study the dynamical behaviour of the BFSO model for values of $x_{10}(0)$ ranging from 1×10^{-6} M to 8×10^{-6} M.

5 Computational details

A popular tool to explore the complexities of dynamical systems is the Lyapunov exponent.⁴² Stability diagrams based on Lyapunov exponents are commonly used to dichotomically sort out periodic from chaotic oscillations. However, the computational cost of constructing such diagrams is relatively high, and their information content is far from the maximal possible. Here, we record the distribution of the stability phases of the peroxidase–oxidase oscillator, as well as their boundaries, using isospike stability diagrams^{17–21} namely using diagrams which, in addition to representing chaotic, present also the number of spikes (local maxima) per period of the periodic oscillations of any variable of interest. Examples of isoperiodic diagrams are given in Fig. 4–6, where colours indicate phases characterized by periodic oscillations while black denotes phases where no periodic oscillations were detected. Isoperiodic diagrams have been found useful in the study of complex systems.^{43–48} For a recent survey about the computation of standard Lyapunov stability diagrams and more fruitful alternatives see ref. 21.

Isoperiodic diagrams are much more informative because they not only discriminate periodicity from chaos similarly to Lyapunov diagrams but, in addition, their colours simultaneously provide detailed cartographic information regarding the number of spikes per period of the periodic oscillations. Isoperiodic diagrams allow one to conveniently visualize how the number of spikes per period unfolds over extended parameter windows when two control parameters are concurrently varied. Although in mathematical flows the period varies continuously, the number of spikes per period varies discretely. Discrete variations allow one to contrast distinct stability

phases more easily, as illustrated by Fig. 4–6 and by 13 additional figures in the ESI.†

To produce the phase diagrams discussed in the next Section, one starts by covering the parameter window of interest with a grid of typically $1200 \times 1200 = 1.44 \times 10^6$ equidistant points. Then, for each grid point, the temporal evolution is determined by integrating numerically eqn (5)–(14) using the standard fourth-order Runge–Kutta algorithm with fixed time-step $h = 0.005$. Integrations were performed horizontally from right to left starting from the initial conditions $x_1 = x_2 = \dots = x_9 = 0$. The initial values of x_{10} acts as an extra control parameter, recorded in each individual stability diagram and in the ESI.† Integrations were done by following the attractor, namely we used the values of x_i obtained at the leftmost end (when finishing the calculation of a horizontal line) to start the calculation for a new horizontal line, after incrementing the parameter vertically. The first 7×10^5 integration steps were discarded as a transient time needed to approach the attractor, with the subsequent 140×10^5 steps used to compute up to 800 extrema (maxima and minima) for all ten variables of the system, checking whether maxima repeated or not.

Our diagrams display the number of spikes per period using a palette of 17 colours. Oscillations with more than 17 spikes are plotted by recycling the 17 basic colours “modulo 17”, namely by assigning them a colour-index given by the remainder of the integer division of the number of peaks by 17. Multiples of 17 are assigned the index 17. Black is used to represent “chaos” *i.e.* lack of numerically detectable periodicity, white and gold mark constant (*i.e.* non-oscillatory) solutions, if any, having respectively non-zero or zero amplitudes of the variable under consideration.

6 Stability diagrams

Fig. 4 shows ten typical stability diagrams obtained, as described above, for a control parameter window where k_9 and k_{12} display the strongest variation. By counting the number of spikes per period of the periodic oscillations, we assigned a colour (shading) to represent the number of spikes found. Black was used to represent lack of numerically detectable periodicity, *i.e.* non-periodic oscillations. This assignment was done for each individual variable x_i , $i = 1, \dots, 10$ in eqn (5)–(14) and for every parameter point of the 1200×1200 grids. The ten individual panels were obtained starting from $x_{10}(0) = 1.5 \times 10^{-6}$ M, representing the initial concentration of Per^{3+} . We determined all stability diagrams, independently of whether or not the variables underlying them may be measured directly in experiments.

Grosso modo, the panels composing Fig. 4 form three groups of stability diagrams, namely (i) x_1 , x_2 , and x_8 , (ii) x_5 , and the larger group formed by (iii) x_3 , x_4 , x_6 , x_7 , x_9 , and x_{10} . However, closer inspection reveals a myriad of small differences among panels in each group. It is worth stressing that isospike diagrams display the number of spikes per period, not the period of the oscillations. The period varies continuously, while

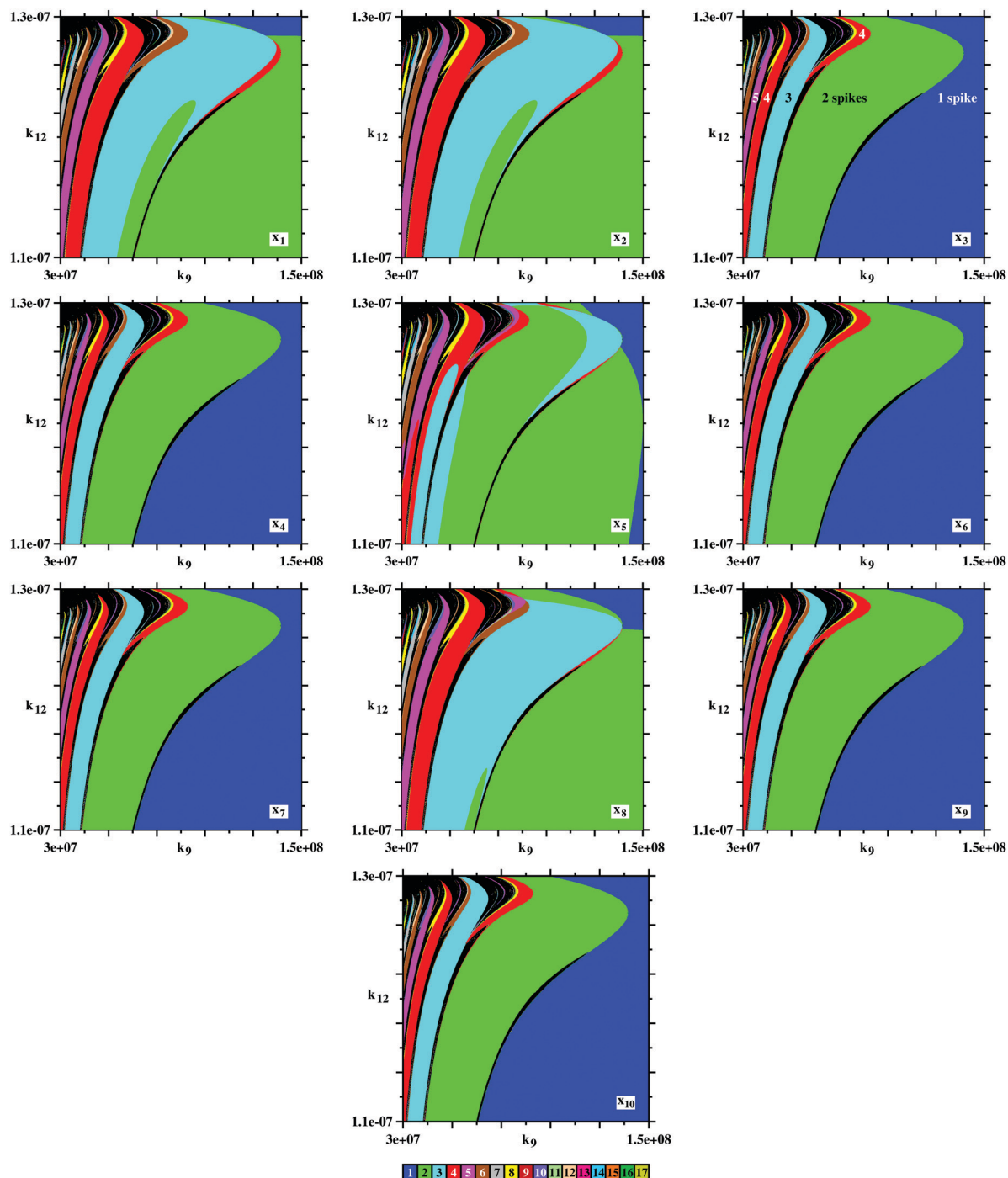


Fig. 4 Stability diagrams representing in colours the number of spikes (local maxima) per period for the ten variables x_i of the model, when fixing the initial condition $x_{10}(0) = 1.5 \times 10^{-6}$ M. The variable x_i for which the isospike diagram is calculated is inserted at the bottom right of each panel. Black denotes chaos, *i.e.* lack of numerically detectable periodicity. The colourbar at the bottom applies to all panels.

the number of spikes varies discontinuously.²¹ For example, the blue domain in Fig. 4 for variables x_3 , x_4 , x_6 , x_7 , x_9 and x_{10} represents oscillations with one spike per period, while much of the corresponding domain for variables x_1 , x_2 , x_5 and x_8 represents oscillations with two spikes per period. However, for all ten variables in this domain corresponds to a simple periodic oscillation in the sense that their phase plot is a one-loop limit cycle.

Although individual phases are different on a finer scale, they reveal relatively similar division of the control parameter windows. It is important to keep in mind that these diagrams are by no means easy to obtain experimentally. But it is quite reassuring to learn that, in essence, their overall agreement is quite satisfactory. For instance, at high values of k_9 (corresponding to a low pH) we observe a period-doubling route to chaos as k_{12} is increased, while at low values of k_9 ,

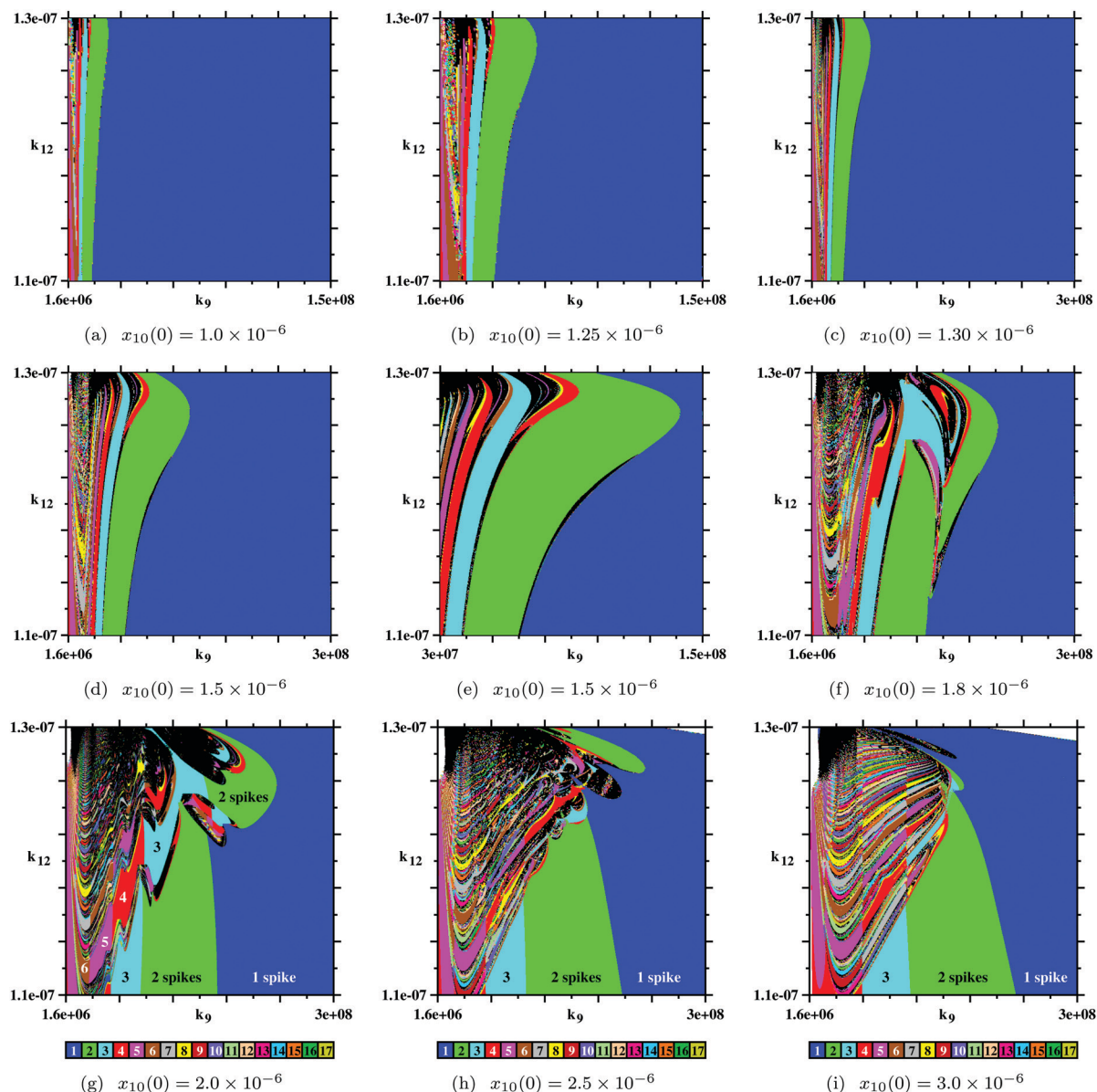


Fig. 5 Evolution observed when counting spikes of x_3 as a function of the initial condition x_{10} (in M). The white regions growing on the upper part of the panels denote phases of non-oscillating zero-amplitude solutions. Panel (e) presents a magnification of a selected region from panel (d). Notice differences in the horizontal scales, used to enhance visualization of details. As indicated on the bottom row, large dark blue phase represent parameters leading to regular oscillations with ones spike per period. The colour coding is the same in all panels.

(corresponding to a high pH) we observe a peak-adding sequence of periodic states culminating in chaos.

In the x_3 panel in Fig. 4, numbers mark the number of spikes per period for the first few major parameter windows. The colourbar, valid for all ten panels, indicates how higher number of spikes were coded, modulo 17. Note that there are two distinct possibilities for transitioning between phases having one and two spikes: transitions may or may not be mediated by a narrow black phase representing non-periodic oscillations. Similar duality of nonchaos-mediated and chaos mediated passages is possible between phases characterized by higher number of spikes. Such dual possibility of transition was previously observed in ref. 41.

How do stability diagrams change when increasing $x_{10}(0)$, namely the initial concentration of Per^{3+} ? Fig. 5 provides an answer, illustrating how diagrams obtained by counting spikes of x_3 vary with $x_{10}(0)$. The variable x_3 , *i.e.* Per^{6+} , was chosen because it is the experimentally best accessible variable. Per^{6+} is one of two dominant redox states (the other is Per^{3+} , namely x_{10}) in the PO reaction and has a distinct absorption peak at 418 nm and it gives a large almost noise-free signal⁴⁹ as opposed to, *e.g.*, the signals from NADH (x_6) or O_2 (x_7) which are relatively noisy. Other experimental variables (corresponding to variables x_1 , x_2 , x_4 , x_5 , x_8 and x_9) cannot be measured, either because their concentrations are extremely low or because they are spectroscopically “silent”. In this, as well as in

all other figures, the large blue regions represent parameters producing regular oscillations with one spike per period.

Manifestly, Fig. 5 shows that stability diagrams do not change significantly from $x_{10}(0) = 1.0 \times 10^{-6}$ M up to about $x_{10}(0) = 1.5 \times 10^{-6}$ M. Beyond this, the otherwise relatively smooth spike phase starts to develop rather intricate structures. In the top portion of the diagrams, the smooth and mild bending turns into a complex phase protruding to the right and acquiring an inner structure. As $x_{10}(0)$ grows more and more, the previously tame phases develop a rather complex mosaic-like covering of spike phases that, while easy to grasp visually from the figure, are difficult to describe briefly with words. For $x_{10}(0) \leq 1.5 \times 10^{-6}$ M the phase diagrams appear as an elongated seemingly well-ordered system of domains of periodic states separated by domains of period-doubled and non-periodic states. At values of 1.5×10^{-6} M $< x_{10}(0) < 3.0 \times 10^{-6}$ M the phase diagrams develop in to a “molten” version of the diagrams obtained at $x_{10}(0) \leq 1.5 \times 10^{-6}$ M. At values of $x_{10}(0) \geq 3.0 \times 10^{-6}$ M the phase diagrams become a patchwork of periodic and non-periodic states enclosed in an almost ellipsoidal structure which again is surrounded by states with few spikes (see below, Fig. 6 and 7).

From the panels at the bottom of Fig. 5 it is possible to recognize a curious phenomenon involving the large stripes corresponding to phases of regular oscillations with 1, 2, and 3 spikes per period. These wide stripes have a clear impact in the

complex mosaic-like phases which exists above the stripes, in the region of larger values of k_{12} . It is important to emphasize that there is no theoretical procedure to anticipate the complicated unfolding of the self-organization of spikes for a given set of coupled nonlinear differential equations. We have not been able to understand why the stripes have such a long-ranging effect in the intricate mosaic of phases which exist above them.

The last panels in Fig. 5 seem to provide evidence that the phases which protrude to the right for $x_{10}(0) = 1.8 \times 10^{-6}$ M, $x_{10}(0) = 2.0 \times 10^{-6}$ M, and $x_{10}(0) = 2.5 \times 10^{-6}$ M, have receded for $x_{10}(0) = 3.0 \times 10^{-6}$ M. This behaviour prompts a natural question: what happens to the mosaic of phases when $x_{10}(0)$ further grows? The answer is given in Fig. 6.

Fig. 6 shows what happens to the stability diagrams obtained by counting spikes of x_3 when the value of $x_{10}(0)$ increases beyond the values presented in Fig. 5. The most significant feature is that the complex mosaic of phases seems to preserve essentially the same topology. It is not difficult to recognize that the structure found for $x_{10}(0) = 4.0 \times 10^{-6}$ M starts to inflate as $x_{10}(0)$ increases continuously while preserving similar topological structure. Conspicuously, the aforementioned long-ranging effects on the intricate mosaic of phases which arise from the large stripes of 2, 3, 4, 5 spikes at the bottom of the panels not only persist but have their influence made remarkably more clearly noticeable.

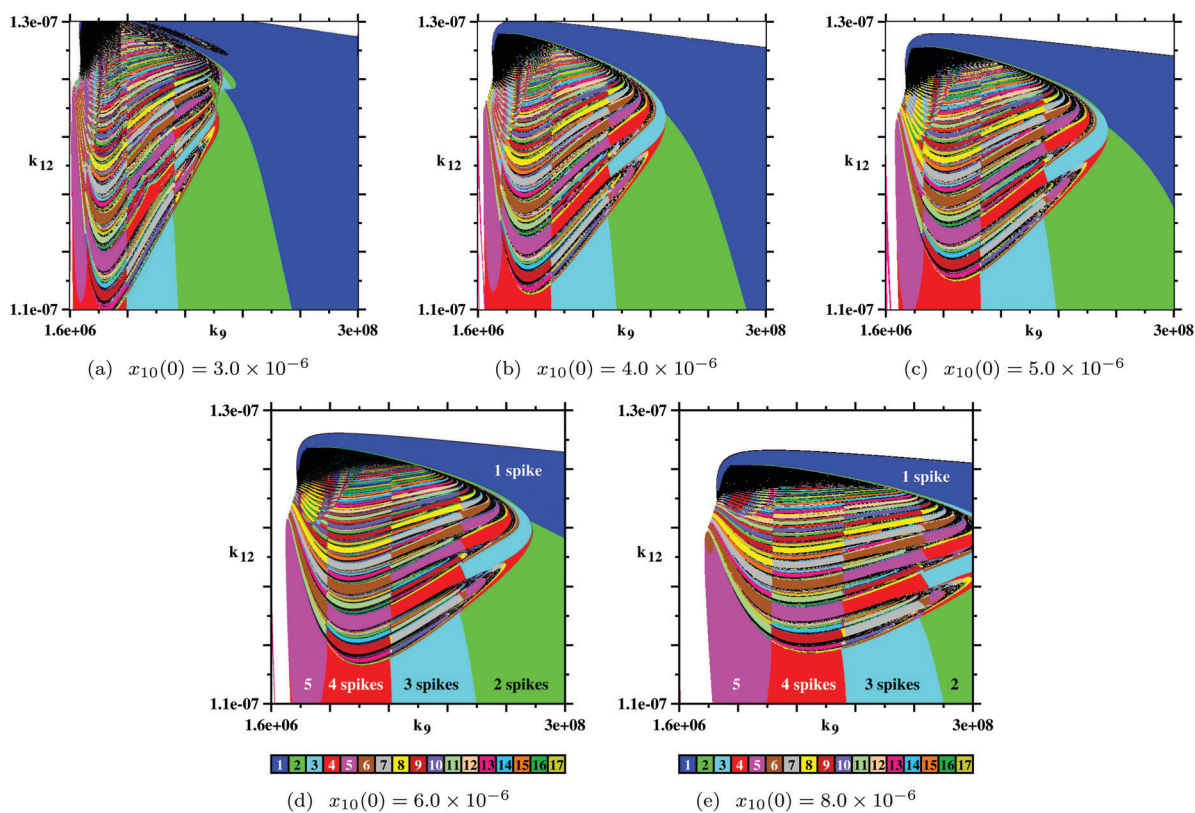


Fig. 6 Crystallization process of the distribution of x_3 spikes observed when x_{10} increases. The complex mosaic of phases remains roughly invariant topologically. The growing white stripes on the top and on the left boundaries denote phases of non-oscillating solutions (fixed points) with zero amplitude. The colour coding is the same in all panels.

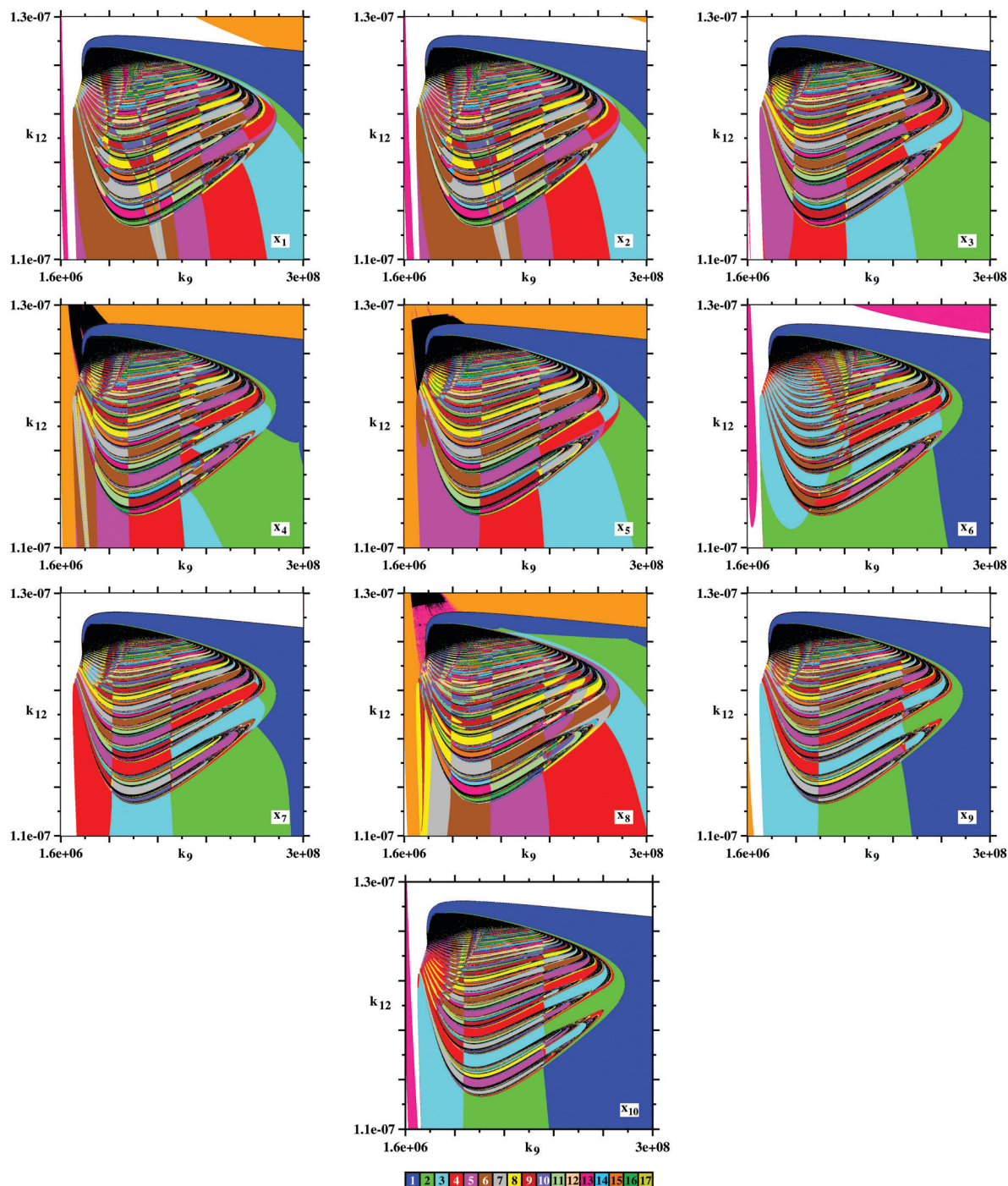


Fig. 7 The structural mosaic crystallization is observed for all ten variables x_i of the model, here shown for $x_{10}(0) = 6.0 \times 10^{-6}$ M. The individual distribution of spike phases depends of the variable used to count the spikes. Stability diagrams for all ten variables and for several additional values of $x_{10}(0)$ are given in the ESI† to this paper. The colourbar of the bottom panel applies to all panels.

Although not every feature of the stability diagrams in Fig. 5 and 6 can be explained in detail, we may use the reaction scheme in Fig. 3 to find out why an increase in $x_{10}(0)$ results in a growth of the phase where complex dynamics is observed: it is known that the black reactions in Fig. 3 will only lead to simple periodic oscillations.^{2,34} It is the red additional reactions, reactions (10) and (11), that provide the model with the ability

to show complex dynamics.^{2,16} Thus, the dynamics exhibited by the BFSO model must be a result of the relative contributions of reactions (6) and (11), and hence the fluxes of these reactions may provide a measure of the complexity observed. We calculated these fluxes at the unstable steady state for changing values of k_9 , k_{12} and $x_{10}(0)$ using the simulation software COPASI.⁵⁰ In this way, we observe that whenever the steady

state flux of reaction (11) is small relative to the steady state flux of reaction (6) (typically less than 5%) the dynamics correspond to a simple periodic oscillation. However, for larger relative contributions of the steady state flux of reaction (11) the dynamics almost always correspond to complex periodic or non-periodic oscillations. As the value of x_{10} increases from 1.0×10^{-6} M to 8.0×10^{-6} M the parameter space spanned by k_9 and k_{12} where the relative contribution of the steady state flux of reaction (11) is larger than 5% increases dramatically and so does the complexity of the dynamics.

To further understand the phase diagrams we may use the fact that the PO reaction is an example of an extended activator-inhibitor system.^{30,51,52} In the terminology of dynamical systems, an activator is a species that destabilizes the current state, once its concentration is increased. By contrast, an inhibitor is defined as a species that prevents an unrestricted increase in the concentration of the activator. Stoichiometric network analysis of the reaction network shows that its structure is surprisingly intricate and contains multiple nested feedback loops.³⁰ These are represented by a core system, that leads to periodic oscillations, and at least three additional positive feedback loops.³⁰ The core system contains a positive and a negative feedback loop. The positive feedback loop consists of the autocatalytic formation of NAD^\bullet radical (x_5) during the reduction of Per^{6+} (x_3) to the native Per^{3+} form of the enzyme (x_{10}). This involves reactions (8), (3) and (4) in Fig. 3. The negative feedback loop preventing an unrestricted accumulation of NAD^\bullet consists of the oxidation of NAD^\bullet by oxygen (O_2) (reaction (5) in Fig. 3).³⁰ The most oxidized form of the enzyme (Per^{6+}) serves as an additional inhibitor, since its concentration may temporarily approach or reach zero. Hence, when all enzyme is converted to its most reduced forms (x_9 and x_{10}), the autocatalytic formation of NAD^\bullet through the sequence of reactions (8), (3), and (4) is interrupted. Therefore, even though Per^{6+} is at the origin of the autocatalytic step, its dynamical function is that of an inhibitor. Note that a similar motif is also found in the reduced Oregonator model for the Belousov-Zhabotinsky reaction, where the reduced form of the metal catalyst also plays the role of the dynamic inhibitor because it limits the autocatalytic step (process B) once it is completely oxidized.⁵³ The oscillatory loop is closed by the oxidation of reduced enzyme species (either Per^{3+} or Per^{2+} , *via* reactions (6) and (11) of Fig. 3, respectively), where the oxidation of Per^{3+} predominates for kinetic reasons (the rate of reaction (6) exceeds that of reaction (11)).

Stoichiometric network analysis revealed that, in addition to the aforementioned core oscillator, the intricate reaction network of the BFSO model (Table 1 and Fig. 3) contains three additional subnetworks, each of them providing positive feedback. These subnetworks are made of the core oscillator comprising the interaction between Per^{6+} , O_2 , and NAD^\bullet , plus their reactions with a fourth species that is not involved in the core system. These 4-variable subnetworks are centred around either Per^{3+} , Per^{2+} , or O_2^- .³⁰ The native enzyme Per^{3+} , namely x_{10} , participates in the first positive feedback loop due to complex interactions with the three reaction partners NAD^\bullet ,

O_2 and Per^{6+} .³⁰ This means that complex periodic or non-periodic oscillations may occur. Combining this feedback loop with the core oscillator results in a 4-variable “ Per^{3+} subnetwork”.³⁰

The second activating subnetwork involves the oxidation of the most reduced form of the enzyme (Per^{2+}) by oxygen to yield Per^{6+} (reaction (11) in Fig. 3). On the one hand, reaction (11) generates Per^{6+} which will positively affect the rate of the autocatalytic step. However, it consumes the inhibitor O_2 , thus providing for a positive feedback. When combining this positive feedback with the core oscillator one obtains a 4-variable “ Per^{2+} subnetwork”.³⁰

The third positive feedback loop is given by the reactions converting O_2 to O_2^- (x_8) and *vice versa* (reactions (5) and (7) in Fig. 3). This loop is a positive feedback, as it actively removes O_2 . The net stoichiometry of reactions (5) and (7) shows that the loop is a net consumer of O_2 , *i.e.*, for each mol of O_2 consumed in the loop, only half a mol of O_2 is produced. Accordingly, the loop has two features that have activating character, namely, (i) a net consumption of O_2 , and (ii) the temporary depletion and time-delayed supply of O_2 by the loop. Combining this positive feedback loop with the core oscillator generates a 4-variable “ O_2^- subnetwork”.³⁰

All three subnetworks contribute to the overall dynamics of the PO reaction. However, due to the comparatively low rates of the oxidation of most reduced enzyme species (Per^{2+}), the Per^{2+} subnetwork involving reaction (11) (Fig. 3), always plays a minor role, especially at low enzyme concentrations as discussed above. By contrast, the other two subnetworks (Per^{3+} and O_2^-),³⁰ involving the oxidation of the native enzyme (Per^{3+}) to coIII through reaction (6) in Fig. 3 and the loop formed by reactions (5) and (7) compete for the NAD^\bullet radicals. At the low enzyme concentrations used in most experiments^{3,10,11,26} ($\leq 1.5 \times 10^{-6}$ M) the reaction of NAD^\bullet with O_2 is kinetically preferred over similar reactions with the enzyme.³⁰

However, as shown above, the relative contributions of the different positive feedback loops to the dynamics of the PO reaction will change with a substantial increase in the initial concentration $x_{10}(0)$ of enzyme. Calculations of the Jacobian matrices for different values of $x_{10}(0)$, again using the COPASI software, enable us to identify two of the three subnetworks listed above: the Per^{2+} and the O_2^- subnetworks, respectively. Not surprisingly, the O_2^- subnetwork dominates at low values of $x_{10}(0)$ while the Per^{2+} subnetwork dominates at high values of $x_{10}(0)$. Hence, the increase in the parameter region, spanned by k_9 and k_{12} , where complex dynamics is observed with increasing $x_{10}(0)$ and the dramatic change in the structure of the stability diagrams may well be due to this passage from one subnetwork to the other.

Are the structural characteristics presented in Fig. 6 a specific property of the distribution of the x_3 spikes represented in the figure, or are they also reproduced when counting spikes for other variables? It turns out that the same mosaic crystallization is detected for all ten variables x_i of the model, as illustrated in Fig. 7 for $x_{10}(0) = 6.0 \times 10^{-6}$ M. The individual distribution of spike phases depends of the variable used to

count them, but there is a remarkable degree of topological invariance among the panels. It is important to observe that, in all our stability diagrams, the inner spikes distribution for the set U representing the union of all phases of periodic oscillations may depend on the variable used to count the spikes. However, the shape and the boundary of U do not depend on the variable used to count the spikes. Furthermore, for any fixed set of parameters, the period measured using every variable of the model is always the same, independently of the number of spikes that the individual variables may have. Thirteen sets of stability diagrams for all ten variables and for a large selection of additional values of $x_{10}(0)$ are presented as ESI† to this paper.

7 Conclusions and outlook

This paper presented a brief review of the Bronnikova–Fedkina–Schaffer–Olsen model of the PO reaction, which is known to reproduce well most of the experimental observations available, and to be rich in dynamical behaviours.⁴¹ Using this model, we computed high-resolution phase diagrams providing a detailed view of the stability phases of the reaction observed when recording the number of spikes per period of the periodic oscillations for all ten variables of the model. This was done for a wide range of the initial concentration $x_{10}(0)$ of the enzyme, including domains for which experimental results are still missing.

A startling characteristic revealed by our phase diagrams is the quite significant and unexpected high-complexity of the distribution of states characterized by different waveforms. Furthermore, the structural complexity of the phase diagrams was found to be strongly dependent of the initial enzyme concentration which, therefore, greatly impacts transitions between periodic states with one spike per period, between a myriad of states with an arbitrary number of spikes per period, as well as between periodic to non-periodic states.

The detailed observations of the PO-reaction dynamics described in the present paper imply very time-consuming experiments to be conducted in the laboratory which, however are feasible *in silico* with high-performance computer clusters. The results of such numerical experiments reported here are truly surprising and difficult to explain mathematically due to the total absence of a proper theoretical framework to anticipate the behaviour of nonlinear sets of differential equations. As an additional byproduct, we mention that the detailed predictions reported here for the dynamical behaviour of the PO-reaction over extended ranges of the initial enzyme concentration open now an objective means of validating experimentally the underlying model and to find out whether or not corrections may eventually be needed.

Conflicts of interest

There are no conflicts of interest to declare.

Acknowledgements

JACG thanks CNPq, Brazil, for support, grant 304719/2015-3. LFO acknowledges the Danish Natural Science Research Council (FNU grant no DFF 4002-00465) and the University of Southern Denmark for financial support. LFO is deeply indebted to Otto E. Rössler for introducing him to the concept of chaos on a visit to Tübingen in early 1976.

References

- 1 H. B. Dunford, *Heme Peroxidases*, Wiley-VCH, Weinheim, 1999.
- 2 A. Scheeline, D. L. Olson, E. P. Williksen, G. A. Horras, M. L. Klein and R. Larter, The peroxidase–oxidase oscillator and its constituent chemistries, *Chem. Rev.*, 1997, **97**, 739–756.
- 3 M. J. B. Hauser, L. F. Olsen, T. V. Bronnikova and W. M. Schaffer, Routes to chaos in the peroxidase–oxidase reaction: Period-doubling and period-adding, *J. Phys. Chem. B*, 1997, **101**, 5075–5083.
- 4 M. J. B. Hauser and L. F. Olsen, The role of naturally occurring phenols in inducing oscillations in the peroxidase–oxidase reaction, *Biochemistry*, 1998, **37**, 2458–2469.
- 5 M. J. B. Hauser and L. F. Olsen, The role of naturally occurring phenols in inducing oscillations in the peroxidase–oxidase reaction, *Biochemistry*, 1998, **37**, 2458–2469.
- 6 H. Degn, Bistability caused by substrate inhibition of peroxidase in an open reaction system, *Nature*, 1968, **217**, 1047–1050.
- 7 I. Yamazaki, K. Yokota and R. Nakajima, Oscillatory oxidations of reduced pyridine nucleotide by peroxidase, *Biochem. Biophys. Res. Commun.*, 1965, **21**, 582–586.
- 8 H. Degn, Compound-3 kinetics and chemiluminescence in oscillatory oxidation reactions catalyzed by horseradish peroxidase, *Biochim. Biophys. Acta*, 1969, **180**, 271–290.
- 9 S. Nakamura, K. Yokota and I. Yamazaki, Sustained oscillations in a lactoperoxidase NADPH and O₂ system, *Nature*, 1969, **222**, 794–795.
- 10 L. F. Olsen and H. Degn, Oscillatory kinetics of peroxidase–oxidase reaction in an open system – experimental and theoretical studies, *Biochim. Biophys. Acta*, 1978, **523**, 321–334.
- 11 L. F. Olsen and H. Degn, Chaos in an enzyme reaction, *Nature*, 1977, **267**, 177–178.
- 12 O. E. Rössler, Chaotic behaviour in simple reaction systems, *Z. Naturforsch., A: Phys. Sci.*, 1976, **31**, 259–264.
- 13 R. A. Schmitz, K. R. Graziani and J. L. Hudson, Experimental evidence of chaotic states in Belousov-Zhabotinskii reaction, *J. Chem. Phys.*, 1977, **67**, 3040–3044.
- 14 R. J. Field, Chaos in the Belousov-Zhabotinsky reaction, *Mod. Phys. Lett. B*, 2015, **29**, 1530015.
- 15 S. K. Scott, *Chemical Chaos*, 2nd edn, International Series of Monographs on Chemistry (Book 24), Oxford University Press, Oxford, 1993.

- 16 T. V. Bronnikova, V. R. Fedkina, W. M. Schaffer and L. F. Olsen, Period-doubling bifurcations and chaos in a detailed model of the peroxidase-oxidase reaction, *J. Phys. Chem.*, 1995, **99**, 9309–9312.
- 17 J. G. Freire and J. A. C. Gallas, Stern–Brocot trees in the periodicity of mixed-mode oscillations, *Phys. Chem. Chem. Phys.*, 2011, **13**, 12191–12198.
- 18 J. G. Freire and J. A. C. Gallas, Stern–Brocot trees in cascades of mixed-mode oscillations and canards in the extended Bonhoeffer–van der Pol and the FitzHugh–Nagumo models of excitable systems, *Phys. Lett. A*, 2011, **375**, 1097–1103.
- 19 M. A. Nascimento, J. A. C. Gallas and H. Varela, Self-organized distribution of periodicity and chaos in an electrochemical oscillator, *Phys. Chem. Chem. Phys.*, 2011, **13**, 441–446.
- 20 M. R. Gallas, M. R. Gallas and J. A. C. Gallas, Distribution of chaos and periodic spikes in a three-cell population model of cancer, *Eur. Phys. J. ST*, 2014, **223**, 2131–2144.
- 21 J. A. C. Gallas, Spiking systematics in some CO₂ laser models, *Adv. At., Mol., Opt. Phys.*, 2016, **65**, 127–191.
- 22 V. R. Fedkina, T. V. Bronnikova and F. I. Ataullakhanov, Phase-space structure for the models of peroxidase-oxidase reaction, *Biofizika*, 1992, **37**(5), 885–894.
- 23 V. R. Fedkina and T. V. Bronnikova, Complex oscillations in peroxidase oxidase reaction, *Biofizika*, 1992, **40**(1), 36–47.
- 24 T. Hauck and F. W. Schneider, Mixed-mode and quasi-periodic oscillations in the peroxidase oxidase reaction, *J. Phys. Chem.*, 1993, **97**, 391–397.
- 25 T. Hauck and F. W. Schneider, Chaos in a Farey sequence through period-doubling in the peroxidase-oxidase reaction, *J. Phys. Chem.*, 1994, **98**, 2072–2077.
- 26 M. J. B. Hauser and L. F. Olsen, Mixed-mode oscillations and homoclinic chaos in an enzyme reaction, *J. Chem. Soc., Faraday Trans.*, 1996, **92**, 2857–2863.
- 27 M. S. Samples, Y. F. Hung and J. Ross, Further experimental studies on the horseradish-peroxidase oxidase reaction, *J. Phys. Chem.*, 1992, **96**, 7338–7342.
- 28 L. F. Olsen, An enzyme reaction with a strange attractor, *Phys. Lett. A*, 1983, **94**, 454–457.
- 29 K. Yokota and I. Yamazaki, Analysis and computer simulation of aerobic oxidation of reduced nicotinamide adenine-dinucleotide catalyzed by horseradish-peroxidase, *Biochemistry*, 1977, **16**, 1913–1920.
- 30 A. Senses, M. J. B. Hauser and M. Eiswirth, Feedback loops for Shilnikov chaos: The peroxidase-oxidase reaction, *J. Chem. Phys.*, 2006, **125**, 014901.
- 31 V. R. Fedkina, F. I. Ataullakhanov and T. V. Bronnikova, Computer simulation of sustained oscillations in peroxidase-oxidase reaction, *Biophys. Chem.*, 1984, **19**, 259–264.
- 32 B. D. Aguda and R. Larter, Sustained oscillations and bistability in a detailed mechanism of the peroxidase oxidase reaction, *J. Am. Chem. Soc.*, 1990, **112**, 2167–2174.
- 33 B. D. Aguda and R. Larter, Periodic chaotic sequences in a detailed mechanism of the peroxidase oxidase reaction, *J. Am. Chem. Soc.*, 1991, **113**, 7913–7916.
- 34 D. L. Olson, E. P. Williksen and A. Scheeline, An experimentally based model of the peroxidase-NADH biochemical oscillator – an enzyme-mediated chemical switch, *J. Am. Chem. Soc.*, 1995, **117**, 2–15.
- 35 C. G. Steinmetz and R. Larter, The quasi-periodic route to chaos in a model of the peroxidase oxidase reaction, *J. Chem. Phys.*, 1991, **94**, 1388–1396.
- 36 M. R. Gallas and J. A. C. Gallas, Nested arithmetic progressions of oscillatory phases in Olsen’s enzyme reaction model, *Chaos*, 2015, **25**, 064603.
- 37 T. V. Bronnikova, W. M. Schaffer, M. J. B. Hauser and L. F. Olsen, Routes to chaos in the peroxidase-oxidase reaction. 2. The fat torus scenario, *J. Phys. Chem. B*, 1998, **102**, 632–640.
- 38 T. V. Bronnikova, W. M. Schaffer and L. F. Olsen, Nonlinear dynamics of the peroxidase-oxidase reaction: I. Bistability and bursting oscillations at low enzyme concentrations, *J. Phys. Chem. B*, 2001, **105**, 310–321.
- 39 T. V. Bronnikova, W. M. Schaffer and L. F. Olsen, Quasiperiodicity in a detailed model of the peroxidase-oxidase reaction, *J. Chem. Phys.*, 1996, **105**, 10849–10859.
- 40 W. M. Schaffer, T. V. Bronnikova and L. F. Olsen, Nonlinear dynamics of the peroxidase-oxidase reaction. II. Compatibility of an extended model with previously reported model-data correspondences, *J. Phys. Chem. B*, 2001, **105**, 5331–5340.
- 41 M. J. B. Hauser and J. A. C. Gallas, Nonchaos-mediated mixed-mode oscillations in an enzyme reaction system, *J. Phys. Chem. Lett.*, 2014, **5**, 4187–4193.
- 42 A. Pikovsky and A. Politi, *Lyapunov Exponents, A Tool to Explore Complex Dynamics*, Cambridge University Press, Cambridge, 2016.
- 43 J. G. Freire, T. Pöschel and J. A. C. Gallas, Stern–Brocot trees in spiking and bursting of sigmoidal maps, *Europhys. Lett.*, 2012, **100**, 48002.
- 44 J. A. Vélez, J. Bragard, L. M. Pérez, A. M. Cabanas, O. J. Suarez, D. Laroze and H. L. Mancini, Periodicity characterization of the nonlinear magnetization dynamics, *Chaos*, 2020, **30**, 093112.
- 45 X. B. Rao, Y. D. Chu, L. Xu, Y. X. Chang and J. G. Zhang, Fractal structures in centrifugal flywheel governor system, *Commun. Nonlinear Sci. Num. Simul.*, 2017, **50**, 330–339.
- 46 L. Xu, Y. D. Chu and Q. Yang, Novel dynamical scenario of the two-stage Colpitts oscillator, *Chaos, Solitons and Fractals*, 2020, **138**, 109998.
- 47 X. B. Rao, X. P. Zhao, J. S. Gao and J. G. Zhang, Self-organization with fast-slow time scale dynamics in a memristor-based Shinriki’s circuit, *Commun. Nonlinear Sci. Num. Simul.*, 2021, **94**, 105569.
- 48 C. S. Rodrigues, C. G. P. dos Santos, C. C. de Miranda, E. Parma, H. Varela and R. Nagao, A numerical investigation of the effect of external resistance and applied potential on the distribution of periodicity and chaos in the anodic dissolution of nickel, *Phys. Chem. Chem. Phys.*, 2020, **22**, 21823–21834.
- 49 M. J. B. Hauser, A. Lunding and L. F. Olsen, On the role of methylene blue in the oscillating peroxidase-oxidase reaction, *Phys. Chem. Chem. Phys.*, 2000, **2**, 1685–1692.

- 50 S. Hoops, S. Sahle, R. Gauges, C. Lee, J. Pahle, N. Simus, M. Singhal, L. Xu, P. Mendes and U. Kummer, COPASI – a complex pathway simulator, *Bioinformatics*, 2006, **22**, 3067–3074.
- 51 I. Schreiber, Y.-F. Hung and J. Ross, Characterization of some oscillatory enzymatic reactions, *J. Phys. Chem.*, 1996, **100**, 8556–8566.
- 52 B. D. Aguda, L. L. Hofmann Frisch and L. F. Olsen, Experimental evidence for the coexistence of oscillatory and steady states in the peroxidase–oxidase reaction, *J. Am. Chem. Soc.*, 1990, **112**, 6652–6656.
- 53 J. J. Tyson and P. C. Fife, Target patterns in a realistic model of the Belousov-Zhabotinskii reaction, *J. Chem. Phys.*, 1980, **73**, 2224–2237.